https://doi.org/10.1016/j.conbuildmat.2024.134892

COMPRESSIVE BEHAVIOR OF FRP TUBULAR COLUMNS WITH RECYCLED CONCRETE LUMPS AND FLOWABLE GROUT

Le Huang[a, b], Tao Yu[a*], Guanzheng Wu[b], Shishun Zhang[c], Hongchao Zhao[d]

[a]*Department of Civil and Environmental Engineering, The Hong Kong Polytechnic University, Hung Hom, Kowloon, Hong Kong, China. Email: tao-cee.yu@polyu.edu.hk*
[b]*School of Civil, Mining & Environmental Engineering, Faculty of Engineering & Information Sciences, University of Wollongong, Australia.*
[c]*School of Civil and Hydraulic Engineering, Huazhong University of Science and Technology, Wuhan, China.*
[d]*School of Geology and Mining Engineering, Xinjiang University, Urumqi, 830000, China*

ABSTRACT

This paper presents a study on the compressive behavior of a novel type of highly deformable hybrid FRP tubular columns. The columns consist of an FRP tube filled with large-size recycled concrete lumps (RCLs) as aggregates and flowable grout as the binding material, and are thus termed FRP-RCL-Grout (F-R-G) columns. The use of large-size RCLs (e.g., up to 63 mm RCLs for 200 mm circular columns) leads to a relatively high recycling ratio and facilitates the manufacturing process. The flowable grout can be easily poured/pumped into the FRP tube, leading to ease of construction, while the FRP tube acts as an effective lateral confining device. The experimental part of the study involved compression tests on F-R-G columns and similar columns for comparison, with the main test variables being the FRP tube thickness, the size of the RCLs, the compressive strength of the concrete for producing RCLs and the WP ratio of the grout. The test results showed that F-R-G columns possess excellent structural behavior including ample ductility, and clarified the effects of the key parameters. In addition, based on the test results, a simple yet accurate model is proposed to predict the strength of F-R-G columns.

KEYWORDS

FRP tube; Hybrid column; Confinement; Recycled concrete lumps; Flowable grout.

1 INTRODUCTION

The conventional way of recycling demolished concrete [1-3], which involves the crushing of concrete into relatively small particles and the subsequent sorting/sieving to obtain recycled coarse aggregate, is a labor- and energy-intensive process. An emerging recycling method initially proposed by [4], in which the demolished concrete is only crushed into large pieces (e.g., with a size larger than 50 mm) of concrete lumps (i.e., recycled concrete lumps or RCLs) for direct use in concrete production, has attracted increasing research attention. Wu's research group has conducted extensive studies on the physical and mechanical properties of RCL-based compound concrete [5-7] and the behavior of various structural members incorporating RCLs [8-10]. These studies have demonstrated the feasibility of using RCL in producing structural concrete, but have also shown that RCL-based compound concrete generally suffers from two issues: (1) the relatively large inhomogeneity of RCLs and the relatively weak bonding at the interface of RCLs and the fresh concrete [8]; (2) the difficulty in mixing RCLs with new fresh concrete to form the compound concrete, which often leads to increased complexity of the construction process [5].

One effective way to address the first deficiency above is to provide a substantial amount of confinement to the RCL-based compound concrete by using it in a confining tube. This was demonstrated by [9-10] who tested RCL-based compound concrete-filled steel tubes, and by [11] who proposed to use the compound concrete in a fibre-reinforced polymer (FRP) confining tube. An FRP confining tube is considered superior to a steel tube for this purpose, as it provides continuously increasing confining pressure due to its linear elastic nature and does not suffer from local buckling due to its

relatively small axial stiffness [12]; FRP also has the additional advantage of being corrosion-resistant.

This paper presents a study to further develop the FRP-confined RCL-based compound concrete columns proposed by [11] by using flowable grout to replace normal fresh concrete, so as to address the second deficiency above of the compound concrete. This simple change significantly facilitates the construction process of the columns: it involves prefilling the FRP tube (stay-in-place formwork) with RCLs (and additional internal longitudinal reinforcement) and then simply pouring/pumping flowable grout into the tube to fill the remaining voids; the grout is generally made by mixing powder with water on site where water is generally available, which can highly reduce the transportation cost; the grout typically has a high water-powder ratio and is thus highly flowable with a low viscosity, which can highly ease the pouring and lead to reduction of labour demands and project timelines; The FRP confining tube typically only contains fibres close to the hoop direction as lateral confinement. The resulting columns are termed herein hybrid FRP-RCL-grout (F-R-G) columns or F-R-G columns. Although the flowable grout material used in this study may lead to a higher material cost, this will not affect the economic efficiency of F-R-G columns due to the reductions in transportations cost, labour demands and project timelines resulting from the use the flowable grout. F-R-G columns may also be considered as a variation of the FRP tubular columns tested by [13] with an infill composed of normal coarse aggregates and high-water material. Like the two column forms investigated in [11] and [13], F-R-G columns are expected to possess many advantages including their high deformation capacity and ease for construction. These columns are therefore particularly suitable for use as compressive members to sustain large deformation such as standing supports in

underground mines [13-14], piles to strengthen weak soil/ground for the foundation of highway/railway or to replace reinforced sandy piles [15-16] and granular piles [17-18]. In this study, experimental tests were carried out on the axial compressive behavior of F-R-G columns. Details of the experimental programme and the obtained test results are presented and analyzed in the subsequent sections, followed by the development of an analytical model to predict the strength of such columns.

2 EXPERIMENTAL PROGRAMME

2.1 Test Specimens

16 specimens in total were built and tested in the experimental programme, consisting of six pairs of F-R-G specimens and two pairs of control specimens; the two specimens in each pair are designed to be nominally identical. The latter included: (1) a pair of grout-filled FRP tube specimens [i.e., F-G specimens without RCLs as shown in Figure 1(b)]; and (2) a pair of unconfined RCL-grout specimens [i.e., R-G specimens without an FRP tube as shown in Figure 1(c)]. Figure 1 shows the configurations of the cross-sections of the three types of test specimens. All the test specimens had the same cross-sectional diameter of 200 mm (excluding the thickness of FRP tube) and the height of 450 mm.

In addition to the specimen type, the key test valuables included: (1) the thickness of FRP tube; (2) the compressive strength of the concrete used to produce RCLs; (3) the size of RCLs; and (4) the water-powder (WP) ratio of grout. The six pairs of F-R-G specimens covered two FRP tube thicknesses (i.e., 1.5 mm and 3.0 mm), normal- and high-strength concrete for producing RCLs, three size combinations of RCLs (i.e., small size, mixed size and large size) and two WP ratios of grout (i.e., 1.25 and 1.5).

The R-G and F-G specimens each cover one combination of the above variables for comparison with the corresponding F-R-G specimens. Table 1 summarizes the key information of all the 16 test specimens.

As shown in Table 1, a "name" is given to each specimen for convenience of reference. For the F-R-G specimens, the name starts with a letter "A" or "B" to indicate the FRP tube thickness ("A" and "B" for 1.5 mm and 3.0 mm tubes, respectively), which is then followed by a letter "N" or "H" to indicate the concrete compressive strength (normal strength and high strength) used for producing RCLs and a letter S", "M", or "L" to represent the size combination of RCLs (i.e., "small size", "mixed size" and "large size"); the subsequent number 1.25 or 1.5 in the name is used to represent the WP ratio of the grout, and the last Roman digit "I" or "II" is used to mark the two nominally identical specimens of each pair. The same naming system is used for the F-G specimens and R-G specimens, except that the name of the former does not include the parts for RCLs while that of the latter does on include the parts for the FRP tube.

2.2 Material Properties

Recycled concrete lumps (RCLs)

The RCLs employed in this project were obtained by crushing concrete cylinders made of ready-mixed commercial concrete. For both the normal-strength and high-strength concrete used in this study for making RCLs, standard cylinders (150 mm × 300 mm) were made and tested under concentric compression to obtain the cylinder compressive strength according to ASTM C39/C39M-21 [19]. The test results show that during the time for testing F-R-G and R-G specimens, the average cylinder compressive strengths of normal- and high-strength RCLs are 25.6 MPa and 80.6 MPa, respectively.

In addition, water absorption tests were conducted in accordance with BS EN 13369:2018 [20] for the RCLs. In the tests, test samples (RCLs) were immersed in water and weighed every 24 hours until the "change in weight" in 24 hours became less than 0.1%; the saturation weight was then deemed to be obtained. After that, the test samples were dried in a well-ventilated oven at a temperature of 105 ℃ until the "change in weight" in 24 hours became less than 0.1%; the dry weight was then obtained. The "weight loss" can be obtained by subtracting the dry weight from the saturation weight, and the "water absorption ratio" can be obtained by dividing the weight loss by the dry weight. The test results show that the water absorption ratios of the normal- and high-strength RCLs are 9.91% and 6.61%, respectively. By dividing the total saturated weight with the total volume of the saturated test samples, the saturation densities of the normal- and high-strength RCLs were found to be 2.28 g/cm^3 and 2.34 g/cm^3, respectively.

Only the RCLs with a size between 20 mm and 63 mm (i.e., based on the size of standard sieves) were used (see Figure 2); 63 mm is considered a "large size" for the FRP tubes (with an inner diameter of 200 mm) used in this study. The size combination of RCLs is a test variable in this study, with the following three cases considered: (1) "small-size" RCLs with the size between 20 mm and 30 mm [see Figure 3(a)], (2) "mixed-size" RCLs with the size between 20 mm and 63 mm [see Figure 3(b)]; and (3) "large-size" RCLs with the size between 50 mm and 63 mm [see Figure 3(c)]. Figure 4 shows the size distribution of the "mixed-size" RCLs. It should be noted although the "small-size" RCLs (20-30 mm) are generally classified as course recycled concrete

157 aggregate in existing studies on recycled aggregate concrete [3], they are termed "RCLs"
158 in this study for ease of reference and discussion.
159
160 For each size combination, the average volume ratio of RCLs in the test specimens was
161 measured by the following method: (1) filling up an FRP hollow tube (200 mm × 450
162 mm) with randomly picked saturated RCLs and recording the mass of the RCLs; (2)
163 calculating the volume ratio of RCLs using their saturation density; (3) repeating (1)
164 and (2) for five times and calculating the average volume ratio of RCLs. The so-
165 obtained volume ratios of RCLs and grout are given in Table 1, which show that the
166 volume ratio of RCLs in a test specimen is hardly affected by their size combinations
167 and the stacking method, and so are amount of grout used in the specimen.
168
169 *Grout material*
170 The grout material used in this study was a type of pumpable commercial chock grout
171 named "CMT grout" provided by MINOVA Australia. CMT grout consists of mainly
172 calcium sulphoaluminate, calcium sulfate, portland cement and slags [21], and is
173 supplied as ready-blended powder can be readily used with the simple addition of water.
174 The properties of CMT grout depends on the WP ratio, which is suggested to be
175 between 1.0 and 2.0 [22]. In this study, two WP ratios (i.e., 1.25 and 1.5) were adopted
176 considering a balance between the gel time and the compressive strength of the grout.
177 This is because although a higher WP ratio leads to a higher flowability and a longer
178 gel-time, it also leads to a lower compressive strength of the grout [22]. For both WP
179 ratios, 50 mm grout cubes were prepared (see Figure 5) and tested under axial
180 compression according to ASTM C942-15 [23], and the compressive strength of the
181 grout cubes ($f_{c,cube}$) at different ages are summarized in Table 2.

FRP tubes

In this study, FRP tubes containing fibres with an angle of $\pm 75°$ to their longitudinal direction were used, and two different tube thicknesses (i.e., 1.5 mm and 3.0 mm) were considered. To measure the hoop tensile elastic modulus and strength of the FRP tubes, two types of the ring spitting tests were conducted: (1) standard ring-splitting tests following ASTM D2290-19a [24] to obtain the hoop strength of the FRP tubes [see Figure 6(a)]; (2) modified ring-splitting tests following [25] Zhang et al. (2020) to measure the hoop elastic modulus of the FRP tubes [see Figure 6(b)]. The key feature of Zhang et al.'s [25] modified ring-splitting tests is to measure hoop strains at the positions 25 mm away from the gap between the two disks so that the bending effect at the gap can be eliminated. The test results show that the FRP tubes had a Young's modulus and a tensile strength of 41.6 GPa and 756.0 MPa, respectively, in the hoop direction, yielding an ultimate hoop strain of 0.0182.

In addition, axial compression tests of hollow FRP tubes were tested to determine their axial compressive properties according to ASTM D2412-11 [26] [see Figure 7(a)]. For each of the two types (1.5 mm and 3.0 mm thick) of FRP tube, three tube specimens with a height of 300 mm were tested. All the specimens failed abruptly by local damage at/close to the end of the tube [see Figure 7(b)]. Figure 8 shows the axial load- strain curves of the six tested FRP hollow tubes. The axial strains in this figure were obtained from the strain gauges applied at the mid-height of each specimen [see Figure 7(a)]. The average axial load capacity of the 1.5 mm and 3.0 mm FRP tubes are 58.0 kN and 121.3 kN, respectively.

2.3 Preparation of Specimens

The preparation of specimens involved placing saturated RCLs into FRP tubes, which were mounted to a framework with their bottom being properly sealed to prevent water leakage, and then pouring flowable grout to fill the FRP tubes. Before the test, the two ends of each specimen were wrapped with three layers of GFRP strips (30 mm width) to avoid premature failure there, and the end surfaces were flattened by capping with high-strength plaster. Figure 9 shows the key steps of fabricating the specimens.

2.4 Test Setup and Instrumentation

All the specimens were tested under compressive axial displacement load using a rate of 0.45 mm/min. Figure 10 shows a typical specimen in test. For each test specimen, the overall axial shortening was measured by two linear variable displacement transducers (LVDTs), and the hoop strains of the FRP tube were measured using four strain gauges evenly distributed around the FRP tube at its mid-height.

3 TEST RESULTS AND DISCUSSIONS

3.1 General Observations

Figure 11(a-b) show the typical failure modes of F-R-G specimens and Figure 11(c) shows that of F-G specimens. It is evident that the failure modes of F-R-G and F-G specimens are similar and have the following two features: (1) major hoop rupture happened to the FRP tube at around the mid-height of the specimen; (2) several horizontal cracks occurred on the FRP tube along its height. The hoop rupture of FRP tube was attributed to the lateral dilation of the infilled material (i.e., grout and RCLs) in the specimens, and the horizontal cracks were due to the cracking of the resin matrix in the FRP tube under large axial deformation. Figure 11(d) shows the failure mode of

232 the two R-G specimens without an FRP tube (i.e., N-M-1.25-I&II); it can been seen
233 that serious spalling of grout and RCLs occurred over the whole height of the specimens.
234
235 After the tests of the two specimens (i.e., A-N-L-1.25-I&II) containing only large-size
236 RCLs [see Figure 3(c)], the FRP tubes were removed to examine the state of the infilled
237 material. As shown in Figure 12, many large-size RCLs had been crushed into smaller
238 pieces under large deformation during the tests.
239
240 **3.2 Effect of FRP Confinement**
241 ***3.2.1 Effect of the presence of FRP tube***
242 Figure 13 compares the axial stress-strain curves of a pair of R-G specimens (i.e., N-
243 M-1.25-I&II) and a pair of F-R-G specimens (A-N-M-1.25-I&II), and the sole
244 difference between these two pairs of specimens is the presence of FRP tubes in the
245 latter. In Figure 13 and hereafter in the paper, the axial strains are calculated from the
246 overall axial shortenings of the specimens obtained from the LVDT, while the axial
247 stresses refer to that of the infilled material and are obtained by dividing the loads it
248 carried with its net cross-section area. The loads carried by the infilled material were
249 obtained by deducting the axial load taken by the FRP tube from the total load given
250 by the testing machines following the approach adopted by Ref. [13]: (1) when the axial
251 strain is smaller than the average ultimate strain of the hollow FRP tubes (i.e., 0.0051
252 for 1.5 mm FRP tube and 0.0056 for 3.0 mm FRP tube, see Figure 8), it is assumed that
253 for the same axial strain, the load carried by the FRP tube and that carried by the hollow
254 FRP tube are the same; (2) when the axial strain is larger than the average ultimate
255 strain, it is assumed that the load carried by the FRP tube becomes constant and is equal
256 to the ultimate load of the hollow FRP tube, considering that the FRP tube in F-R-G

(and F-G) specimens is well supported by the infilled material. Figure 14 shows the assumed axial load-strain curves of the 1.5 mm and 3.0 mm FRP tubes in F-R-G and F-G specimens.

Figure 13 evidently shows that the axial stress-strain curves of the R-G specimens are similar to that of unconfined concrete, while the curves of the F-R-G specimens are similar to that of typical FRP-confined concrete. The latter consists of three different segments: a linearly ascending initial segment, a smooth nonlinear transition segment and an approximately linear final ascending segment. Similar to FRP-confined concrete, the three segments correspond to the initial elastic stage, the stage when significant damage of the infilled material started to occur, and the final stage when the FRP confinement was effectively activated.

For normal concrete, it has been well established that the stress at the start of transition segment of FRP-confined concrete is approximately equal to the strength of unconfined concrete [27]. However, Figure 13 shows that the transition stress of F-R-G specimens is significantly higher than (i.e., around two times) the strength of the corresponding R-G specimens without FRP confinement. This is believed to be due to the highly inhomogeneous nature of the R-G material as a result of the random distribution of RCLs and the significant strength difference between the RCLs and the grout. As clearly shown in the photos of the failure mode (Figure 11d), all the R-G specimens tested in this study failed by premature separation (cracking) between RCLs and grout followed by spalling of grout and falling of RCLs. It is not difficult to understand that the premature separation (cracking) between RCLs and grout is due to (1) the non-uniform stress distribution (e.g., stress concentration) over the column section due to

the inhomogeneous nature of R-G material and (2) the weak bond between RCLs and grout due to their remarkable different strength. However, the above premature failure mode will not happen to the R-G materials in F-R-G specimens due to the confinement effect of the FRP tube. This is the reason for the noteworthy disparity between F-R-G specimens and R-G specimens shown in Figure 13.

In addition to the above beneficial effect of FRP confinement, it also plays the same role that it does for normal concrete [13, 28-30], as reflected by the final approximately linear segment of the stress-strain curve (Figure 13), leading to significantly enhanced ultimate axial stress and strain. Notably, the strength of F-R-G specimens is around seven times that of the corresponding R-G specimens, while the ultimate axial strain of the former is around 13 times that of the latter.

In addition, it can be seen from Figure 13 that the axial stress strain curves of the two nominally identical specimens in each pair (i.e., N-M-1.25-I and N-M-1.25-II; A-N-M-1.25-I and A-N-M-1.25-II) are nearly the same. This indicates that the difference in staking of RCLs in the specimens has little effect on the compressive behavior of the specimens. Similar observations can be found for all the other test specimens as shown in relevant figures presented latter on.

3.2.2 Effect of the FRP tube thickness

Figure 15 shows the comparison of the axial stress-strain curves of two pairs of F-R-G specimens (i.e., A-N-M-1.25-I&II and B-N-M-1.25-I&II). The sole difference between these two pairs of specimens is the FRP tube thickness (i.e., 1.5 mm and 3.0 mm, respectively). It is evident from Figure 15 that in the early loading stage (with an axial

307 strain smaller than 0.0055), the two pairs of curves nearly overlaps with each other,
308 suggesting that the FRP confinement has marginal effect on the curves in this stage.
309 When the axial strain becomes larger, the curves of the specimens with a 3.0 mm FRP
310 tube become increasingly higher than their counterparts with a 1.5 mm FRP tube. While
311 the curves of the F-R-G specimens all feature an approximately bilinear shape, those of
312 the specimens with a thicker FRP tube have a steeper and longer ascending second
313 linear portion; this is similar to the observations on the behavior of FRP-confined
314 normal concrete [29]. Furthermore, it is evident from Figure 15 that the variation of
315 thickness of the FRP tube has just a minor effect on the transition stress between the
316 two approximately linear portions of the curves.
317
318 To further study the difference between the confinements of the 1.5 mm and 3.0 mm
319 thick FRP tubes, Figure 16(a) compares the hoop strain-axial strain curves of the two
320 pairs of specimens. In this paper, the FRP hoop strains are calculated using the data
321 from the four strain gauges applied at the mid-height of the FRP tube. Based on the data
322 in Figure 16(a), Figure 16(b) shows the relationships between the confining pressure
323 and axial strain for the four specimens. It is evidently indicated that at a given axial
324 strain, the 3.0 mm FRP tube has a smaller hoop strain [see Figure 16(a)] but provides a
325 higher confining pressure [see Figure 16(b)] than the 1.5 mm FRP tube; the distinction
326 between the two pairs of curves tends to increase with axial strain. Figure 16(a) also
327 shows that for a thicker FRP tube, the hoop strain increases less rapidly with the axial
328 strain, and thus leads to a higher ultimate axial strain for a certain rupture strain (e.g.,
329 for the same FRP material). Figure 16(b) explains the reason why a thicker FRP tube
330 leads to a higher axial stress-strain curves of the specimens (see Figure 15). The above

observations are generally similar to those reported for FRP-confined normal concrete columns [28-30].

3.3 Effect of RCLs

3.3.1 Effect of the presence of RCLs

Figure 17 compares the axial stress-axial strain curves and hoop strain-axial strain curves of two pairs of specimens: a pair of F-G specimens (i.e., A-1.25-I&II) and a pair of F-R-G specimens (i.e., A-N-M-1.25-I&II); the sole difference between the two pairs is the infilled materials: the F-G specimens were filled with 100% grout, while the F-R-G specimens were filled with 57.5% grout and 42.5% RCLs (by volume, see Table 1).

By observing the axial stress-strain curves in Figure 17(a), it can be seen that: (1) the initial portions of the two pairs of curves almost overlap with each other; (2) after an axial strain of around 0.02, the axial stress of the F-R-G specimens (A-N-M-1.25-I&II) increases approximately linearly at a rate smaller than their initial stiffness (i.e., the curves showing a second linear portion), while the curves of the F-G specimens exhibit a nonlinear shape with the axial stress increasing at a gradually decreasing rate, leading to increasingly large difference between the two pairs of curves. The above observation is believed to be at least partially due to the different lateral expansion behavior of the two types of infilled materials, as shown in Figure 17(b). The figure evidently shows that when the axial strain is larger than 0.02, the hoop strain of F-G specimens tends to become gradually smaller than that of the corresponding F-R-G specimens, suggesting that the lateral dilation of, and thus the lateral confinement received by the former is increasingly smaller than the latter. Such differences may be attributed to the

significantly higher WP ratio (i.e., 1.25 for the specimens shown in Figure 17) and the resulting more porous microstructure of the grout, compared with the RCLs. For the same reason, it may be expected that the effect of confining pressure on the strength enhancement is less pronounced for the grout than for the grout-RCL compound material.

3.3.2 Effect of the size of RCLs

Figure 18 compares the axial stress-strain curves and hoop strain-axial strain curves of three pairs of F-R-G specimens (i.e., A-N-S-1.25-I&II; A-N-M-1.25-I&II and A-N-L-1.25-I&II), with the sole difference between them being the size combinations of the employed RCLs (i.e., small-size, mixed-size and large-size RCLs, respectively, see Table 1). It is evident from Figures 18(a) and 18(b) that the three pairs of curves are very close to each other, suggesting that the size (combinations) of RCLs, with the range examined in this study, has little effect on the axial stress-strain and lateral dilation behavior of F-R-G specimens. It is also noted that despite the difference in the size of RCLs, the volume ratio of RCLs in the three pairs of specimens is similar (i.e., around 42%, see Table 1). Therefore, the difference in these specimens lies mainly in the inhomogeneity of the compound infilled material (i.e., RCLs and grout). As explained above, the extent of such inhomogeneity may affect the behavior of unconfined specimens, but its effect can be effectively mitigated or eliminated by the confinement from the FRP tube; similar points have also been made by [11] on FRP-confined compound concrete with fresh concrete and RCLs.

3.3.3 Effect of the compressive strength of RCLs

Figure 19 compares the axial stress-strain curves and hoop strain-axial strain curves of two pairs of F-R-G specimens (A-N-M-1.25-I&II and A-H-M-1.25-I&II), with the sole difference between them being the compressive strength of concrete used to make RCLs (i.e., 25.6 MPa and 80.6 MPa, respectively). As shown in Figure 19(a), for a given axial strain, the axial stress of the specimens with high-strength RCLs is only slightly higher (by around 5%) than their counterparts with normal-strength RCLs, while Figure 19(b) shows that there is no remarkable distinction between the lateral dilation behavior of the two pair of specimens. This is not a surprise as the strength of the grout (i.e., 11.9 MPa, see Table 2) is significantly lower than both RCLs, so that the grout is the weak link in the system and plays a dominant role on the compressive damage and lateral expansion behavior of the F-B-G specimens

3.4 Effect of the WP Ratio of the Grout

Figure 20 compares the axial stress-strain curves and hoop strain-axial strain curves of two pairs of F-R-G specimens (A-N-M-1.25-I&II and A-N-M-1.5-I&II), with the sole difference between them being the WP ratio of the grout used (i.e., 1.25 and 1.5, respectively). While the axial stress-strain curves of both pairs of specimens feature an approximately bilinear shape, Figure 20(a) shows that the increase of WP ratio of grout from 1.25 to 1.5 leads to a significant decrease in: (1) the initial stiffness of the specimens; (2) the transition stress between the two linear portions; (3) the slope of the second linear portion; and (4) the ultimate axial stress. The first two differences above indicate that the unconfined properties (stiffness and strength) of the grout-RCL compound material are significantly affected by the WP ratio of grout; this is consistent with the compressive test results of grout cubes given in Table 2 which shows that the

compressive strength of the grout with a WP ratio of 1.25 is 39.5% higher than its counterpart with a WP ratio of 1.5. On the other hand, the last two differences above depend largely on the FRP confinement which is substantially affected by the lateral expansion of the infilled material. The comparison of hoop strain-axial strain curves in Figure 20(b) shows that when the axial strain is larger than 0.015, the lateral expansion of specimens A-N-M-1.25-I&II is remarkably higher than that of A-N-M-1.5-I&II, leading to significantly higher confining pressure for the former at a given axial strain. This remarkable difference in the lateral expansion explains the stiffer second-stage behavior of the specimens with a lower WP ratio (1.25) of grout, and may be attributed to the denser microstructure of such grout.

4 STRENGTH MODEL FOR F-R-G COLUMNS

It has been well established by existing studies [27, 31] that the axial strength of FRP-confined concrete f_{cc} in a circular column may be related to the lateral confining pressure using the following equations:

$$f_{cc} = f_{c0} + kf_l \tag{1}$$

$$f_l = E_f t_f \varepsilon_{fl} / R \tag{2}$$

where f_{c0} is the cylinder strength of unconfined concrete, k is a constant and f_l is the lateral confining pressure provided by FRP; E_f, t_f and ε_{fl} are the hoop elastic modulus, the thickness and the hoop strain of FRP, respectively; R is the radius of the circular column.

Similar to FRP-confined normal concrete with sufficient confinement, the stress-strain curves of the F-R-G specimens feature an approximately bilinear shape with a second ascending branch [see Figures 15, 18(a), 19(a) and 20(a)]. It is thus expected that Eqs. 1 and 2 may also be applied to F-R-G columns for their confined strength. Therefore, a regression analysis based on the present test results was conducted to obtain the constant k in Eq. 1 for the infill material in F-R-G columns. In doing so, seven points were extracted from the experimental stress-strain curve of each F-R-G specimen to generate a test database; the seven points represent different confinement levels, and the confining pressure at each point was calculated by Eq. 2 using the corresponding experimental lateral strain. The so-obtained data points are plotted in Figure 21, where it is evident that the points falls into two sets: one with the WP ratio of 1.25 and the other with the WP ratio of 1.5. It is also evident that both sets of data show a linear pattern, demonstrating the validity of Eq. 1 for F-R-G columns. The best-fit lines for the two sets of data are also plotted in Figure 21 together with the corresponding liner equation, where the slope of the lines represents the value of k in Eq.1. It is evident that for both WP ratios, k can be taken as the same value of 1.7.

The intercept of the best-fit lines with the stress axis represents the unconfined strength (f_{c0}) in Eq. 1; these numbers (i.e., 15.0 MPa and 11.0 MPa for the infill material with WP ratios of 1.25 and 1.50, respectively, see Figure 21) are shown to be significantly higher than the compressive strength of the corresponding grout cubes (see Table 2), although the failure of the unconfined infill material in such columns generally occurs within the grout due to its relatively low strength compared with the RCLs. The lower compressive strengths of grout cubes are believed to be due to the brittle nature of the grout, which makes it prone to internal defects when being tested without confinement;

453 the effects of internal defects, however, can be significantly reduced by providing a
454 small amount of confinement which allows the stress redistribution within the material.
455 Based on the test results, it appears that an enhancement factor of 1.30 may reflect the
456 enhancement of f_{c0} in F-R-G columns compared with that of standard grout cubes for
457 both WP ratios of 1.25 and 1.50 (see Table 2). Nevertheless, it should also be noted that
458 this enhancement factor (i.e., 1.30) is based on the limited test results and its value may
459 be adjusted when more test results become available.
460
461 With the above discussion, the following equation based on Eq. 1 may be used for
462 predicting the confined strength of the infilled material in F-R-G columns:
463
464 $$f_{cc} = f_{c0} + 1.7 f_l \quad (3)$$
465
466 where f_l can be calculated using Eq. 2 and f_{c0} can be taken as 1.30 times the strength
467 from standard cube tests of the grout (see Table 2).
468
469 **5 CONCLUSIONS AND FUTURE STUDIES**
470 In this study, the compressive behavior of a new type of hybrid columns (F-R-G
471 columns) incorporating an FRP confining tube, recycled concrete lumps (RCLs) and
472 flowable grout with a high water-powder ratio was investigated, and a strength model
473 was proposed for such columns with the confinement effect of the FRP tube being
474 properly considered. The following conclusions can be drawn from this study:
475 (1) The presence of the FRP tube can significantly increase the compressive
476 strength (e.g., by around 400% for 1.5 mm FRP tube in this study) and the

deformation capacity (e.g., by around 1100% for 1.5 mm FRP tube in this study) of the compound grout-RCL material in F-R-G columns.

(2) The increase of FRP tube thickness can remarkably increase the lateral confinement provided by the FRP tube and thus lead to appreciable increases in both the compressive strength and ultimate axial strain of the columns.

(3) The presence of RCLs tends to increase the lateral dilation of F-R-G columns for a given axial strain, leading to an increased level of FRP confinement.

(4) The variation of the size of RCLs has marginal effects on the compressive behavior of F-R-G columns.

(5) The variation of the compressive strength of RCLs from 25.6 MPa to 80.6 MPa has marginal effects on the compressive behavior of the F-R-G columns.

(6) The increase of the WP ratio of grout (e.g., from 1.25 to 1.5 in this study) can lead to a significant reduction of the compressive strength of F-R-G columns and a significant increase of their ultimate axial strain.

(7) The proposed strength model captures the effects of FRP confinement and can provide close prediction of the present test results of F-R-G columns, while it may be verified or refined when more test results become available.

(8) The following two disadvantages of F-R-G columns should be noted: (i) the proposed F-R-G columns may mainly be used to support compression load as they have no tensile reinforcement and thus little tensile or flexural resistance; (ii) the CMT grout generally has an initial stiffness smaller than that of concrete, thus in practice the stiffness of F-R-G columns should be properly designed.

The following are some important topics to be covered in future studies on F-R-G columns: (1) the crushing resistance and soundness of RCLs should be measured to

further evaluate the properties of RCLs; (2) accurate models should be proposed to predict the axial stress-strain behaviour of F-R-G columns; (3) the behaviour of the inter-surface zone (ITZ) between RCLs and grout in F-R-G specimens should be further studied to deeply understand the mechanism of the interaction between them.

ACKNOWLEDGEMENT

The authors gratefully acknowledge the financial support provided by the Hong Kong Research Grants Council (Project No: 15222321), The Hong Kong Polytechnic University (1-BE38) and the Australian Research Council (Project ID: DP170102992). The authors also thank MINOVA (Australia) for providing the CMT grout used in this study.

DATA AVAILABILITY

Data will be made available on request.

REFERENCES

[1] Hansen, T.C., ed. Recycling of Demolished Concrete and Masonry. CRC Press 1992.

[2] Poon, C.S., Kou, S.C. and Lam, L. Use of recycled aggregates in molded concrete bricks and blocks. Construction and Building Materials 2002; 16(5):281-289.

[3] Xiao, J., Li, W., Fan, Y. and Huang, X. An overview of study on recycled aggregate concrete in China (1996-2011). Construction and Building Materials 2012; 31:364-383.

[4] Wu, B., Liu, Q.X., Liu, W. and Xu, Z. Primary study on recycled-concrete-segment filled steel tubular members. Earthquake Resistant Engineering and Retrofitting 2008; 30(4):120-124. (In Chinese)

526 [5] Wu, B., Liu, C. and Wu, Y. Compressive behaviors of cylindrical concrete
527 specimens made of demolished concrete blocks and fresh concrete. Construction and
528 Building Materials 2014; 53:118-130.

529 [6] Wu, B., Zhang, S. and Yang, Y. Compressive behaviors of cubes and cylinders
530 made of normal-strength demolished concrete blocks and high-strength fresh
531 concrete. Construction and Building Materials 2015; 78:342-353.

532 [7] Wu, B. and Yan, J. Influences of size and shape of demolished concrete lumps on
533 compressive behavior of compound concrete. Construction and Building Materials
534 2021; 269:121317.

535 [8] Wu, B., Xu, Z., Ma, Z.J., Liu, Q. and Liu, W. Behavior of reinforced concrete beams
536 filled with demolished concrete lumps. Structural Engineering and Mechanics: An
537 International Journal 2011; 40(3):411-429.

538 [9] Wu, B., Zhao, X.Y. and Zhang, J.S. Cyclic behavior of thin-walled square steel
539 tubular columns filled with demolished concrete lumps and fresh concrete. Journal
540 of Constructional Steel Research 2012; 77:69-81.

541 [10] Wu, B., Zhao, X.Y., Zhang, J.S. and Yang, Y. Cyclic testing of thin-walled circular
542 steel tubular columns filled with demolished concrete blocks and fresh
543 concrete. Thin-Walled Structures 2013; 66:50-61.

544 [11] Teng, J.G., Zhao, J.L., Yu, T., Li, L.J. and Guo, Y.C. Behavior of FRP-confined
545 compound concrete containing recycled concrete lumps. Journal of Composites for
546 Construction 2016; 20(1):04015038.

547 [12] Li, Y.L., Teng, J.G., Zhao, X.L. and Raman, R.S. Theoretical model for seawater
548 and sea sand concrete-filled circular FRP tubular stub columns under axial
549 compression. Engineering Structures 2018; 160:71-84.

[13] Yu, T., Zhao, H., Ren, T. and Remennikov, A. Novel hybrid FRP tubular columns with large deformation capacity: Concept and behaviour. Composite Structures 2019; 212:500-512.

[14] Barczak T. An overview of standing roof support practices and developments in the United States. Proceedings of the Third South African Rock Engineering Symposium. Johannesburg, Republic of South Africa: South African Institute of Mining and Metallurgy 2005; 301-334.

[15] Tatyana, M., Alexander, N. and Anastasia, C. Reinforced sandy piles for low-rise buildings. Procedia Engineering 2015; 117:239-245.

[16] Maltseva, T., Nabokov, A., Novikov, Y. and Sokolov, V. The method of calculating the settlement of weak ground strengthened with the reinforced sandy piles. In MATEC Web of Conferences 2016; 73:01015.

[17] Samadhiya, N., Maheshwari, P., Zsaki, A., Basu, P. and Kundu, A. Strengthening of clay by geogrid reinforced granular pile. International Journal of Geotechnical Engineering 2009; 3(3):377-386.

[18] Abhishek, S.V., Rajyalakshmi, K. and Madhav, M.R. Engineering of ground with granular piles: a critical review. International Journal of Geotechnical Engineering 2016; 10(4):337-357.

[19] ASTM C39/C39M-21. Standard Test Method for Compressive Strength of Cylindrical Concrete Specimens. West Conshohocken, PA: American Society for Testing Material; 2021.

[20] BS EN 13369:2018. Common rules for precast concrete products. British standard Institution, London; 2018.

[21] Minova. Safety Dada Sheet: CMT grout. Sydney, Australia; 2020.

574 [22] Minova. Technical Dada Sheet: CMT grout. Sydney, Australia; 2020.

575 [23] ASTM C942-15. Standard test method for compressive strength of grouts for
576 preplaced aggregate concrete in the laboratory. West Conshohocken, PA: American
577 Society for Testing Material; 2015.

578 [24] ASTM D2290-19a. Standard test method for apparent hoop tensile strength of
579 plastic or reinforced plastic pipe. West Conshohocken, PA: American Society for
580 Testing Material; 2019.

581 [25] Zhang, B., Zhao, J.L., Huang, T., Zhang, N.Y., Zhang, Y.J. and Hu, X.M. Effect
582 of fiber angles on hybrid fiber-reinforced polymer–concrete–steel double-skin
583 tubular columns under monotonic axial compression. Advances in Structural
584 Engineering 2020; 23(7):1487-1504.

585 [26] ASTM D2412-11. Standard test method for determination of external loading
586 characteristics of plastic pipe by parallel-plate loading. West Conshohocken, PA:
587 American Society for Testing Material; 2011.

588 [27] Lam, L. and Teng, J.G. Design-oriented stress–strain model for FRP-confined
589 concrete. Construction and Building Materials 2003; 17(6-7):471-489.

590 [28] Mirmiran, A. and Shahawy, M. Behavior of concrete columns confined by fiber
591 composites. Journal of Structural Engineering 1997; 123(5):583-590.

592 [29] Teng, J., Huang, Y.L., Lam, L. and Ye, L.P. Theoretical model for fiber-reinforced
593 polymer-confined concrete. Journal of composites for construction 2007; 11(2):201-
594 210.

595 [30] Huang, L., Yu, T., Zhang, S.S. and Wang, Z.Y. FRP-confined concrete-encased
596 cross-shaped steel columns: Concept and behaviour. Engineering Structures 2017;
597 152:348-358.

598 [31] Ozbakkaloglu, T., Lim, J.C. and Vincent, T. FRP-confined concrete in circular
599 sections: Review and assessment of stress–strain models. Engineering Structures
600 2013; 49:1068-1088.

601

Table 1 Test matrix

Specimen name		Height/ Diameter (mm)	Compressive Strength of RCLs (MPa)	Size of RCLs (mm)	FRP tube thickness (mm)	WP ratio	Volume ratio of grout (%)	Volume ratio of RCLs (%)
A-1.25		450/200	N/A	N/A	1.5	1.25	100	0
N-M-1.25			25.6	Mixed size (20-63)	N/A	1.25	57.5	42.5
A-N-S-1.25			25.6	Small size (20-30)	1.5	1.25	57.3	42.7
A-N-L-1.25				Large size (53-63)	1.5	1.25	58.2	41.8
A-N-M-1.25				Mixed size (20-63)	1.5	1.25	57.5	42.5
A-N-M-1.5				Mixed size (20-63)	1.5	1.50	57.5	42.5
B-N-M-1.25				Mixed size (20-63)	3.0	1.25	57.5	42.5
A-H-M-1.25			80.6	Mixed size (20-63)	1.5	1.25	57.5	42.5

Table 2. Compressive strength of GMT grout cubes ($f_{c,cube}$).

WP ratio	Compressive strength of GMT grout cubes $f_{c,cube}$ (MPa)		
	7-day	28-day	Test-time
1.25	7.9	11.3	11.9
1.50	5.8	8.1	8.3

Table 3. Key results of test specimens.

Specimens	*Axial strength (MPa)	*Average axial strength (MPa)	Ultimate axial strain	Average ultimate axial strain	Ultimate FRP hoop strain	Average ultimate FRP hoop strain
N-M-1.25-I	5.6	5.8	0.0037	0.0040	N/A	N/A
N-M-1.25-II	6.0		0.0042			
A-1.25-I	26.5	26.3	0.0461	0.0470	0.0152	0.0138
A-1.25-II	26.1		0.0479		0.0123	
A-N-S-1.25-I	29.7	29.9	0.0454	0.0474	0.0145	0.0152
A-N-S-1.25-II	30.0		0.0493		0.0159	
A-N-L-1.25-I	31.5	31.8	0.0493	0.0501	0.0173	0.0167
A-N-L-1.25-II	32.0		0.0509		0.0161	
A-N-M-1.25-I	31.6	32.2	0.0480	0.0519	0.0153	0.0161
A-N-M-1.25-II	32.8		0.0557		0.0169	
A-N-M-1.5-I	25.0	25.0	0.0579	0.0594	0.0128	0.0139
A-N-M-1.5-II	25.0		0.0608		0.0150	
B-N-M-1.25-I	44.2	43.2	0.0735	0.0700	0.0163	0.0160
B-N-M-1.25-II	42.1		0.0665		0.0157	
A-H-M-1.25-I	33.7	33.3	0.0466	0.0468	0.0146	0.0153
A-H-M-1.25-II	32.9		0.0469		0.0159	

*For Specimens with FRP tubes, the axial strength value does not include the contribution of the FRP tube.

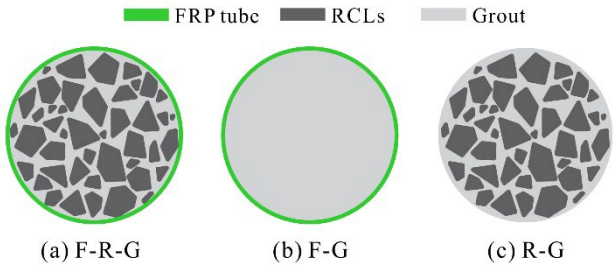

Figure 1. Cross-sectional configurations of the three types of specimens.

Figure 2. RCLs obtained by crushing concrete columns.

(a) (b) (c)

Figure 3. Photos of RCLs of different size combination: (a) small size, (b) mixed size and (c) large size.

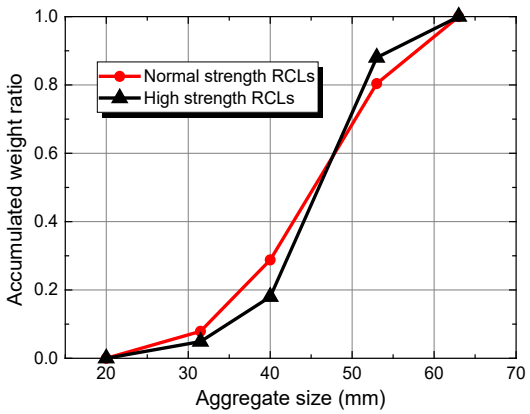

Figure 4. Size distribution of the normal strength and high strength mixed-size RCLs.

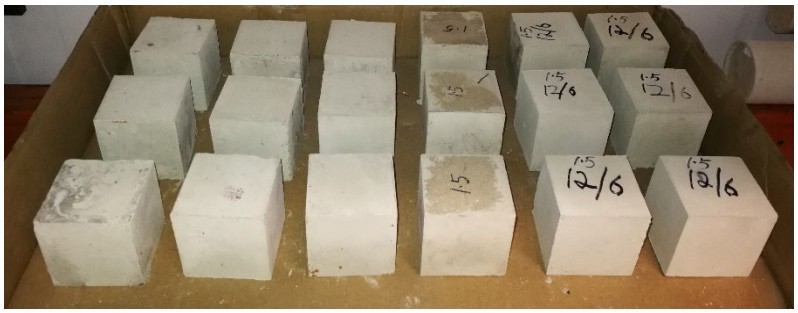

Figure 5. CMT grout cubes for axial compression tests.

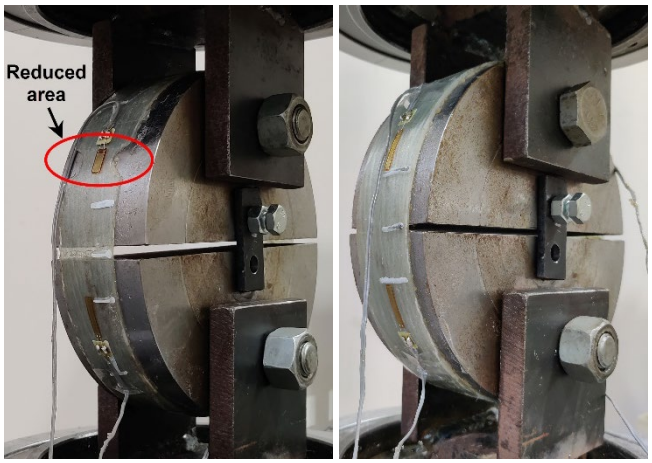

(a) (b)

Figure 6. Ring splitting test of FRP tubes: (a) following ASDM D2290-19a and (b) following Zhang et al. 2020 [25].

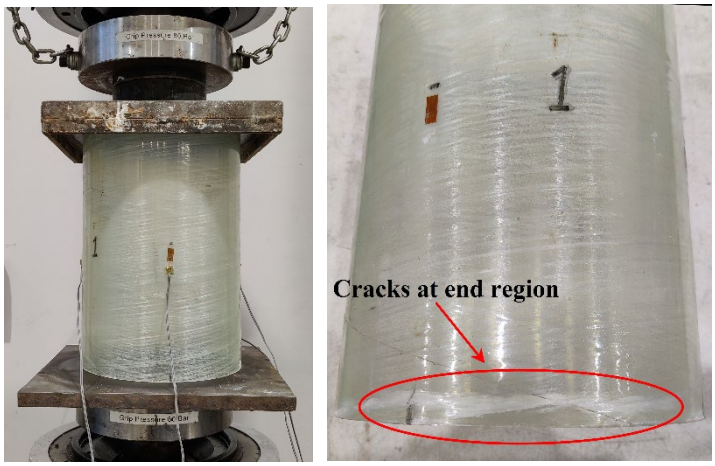

(a) (b)

Figure 7. Compression test of hollow FRP tubes: (a) test setup; (b) typical failure mode.

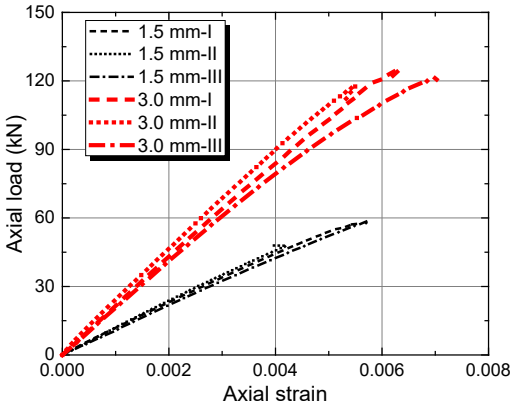

Figure 8. Axial load-strain curves of hollow FRP tubes under axial compression

(a) (b) (c)

Figure 9. Preparation of specimens: (a) filling FRP tubes with RCLs; (b) pouring grout; (c) curing of test specimens.

Figure 10. Test setup for column specimens.

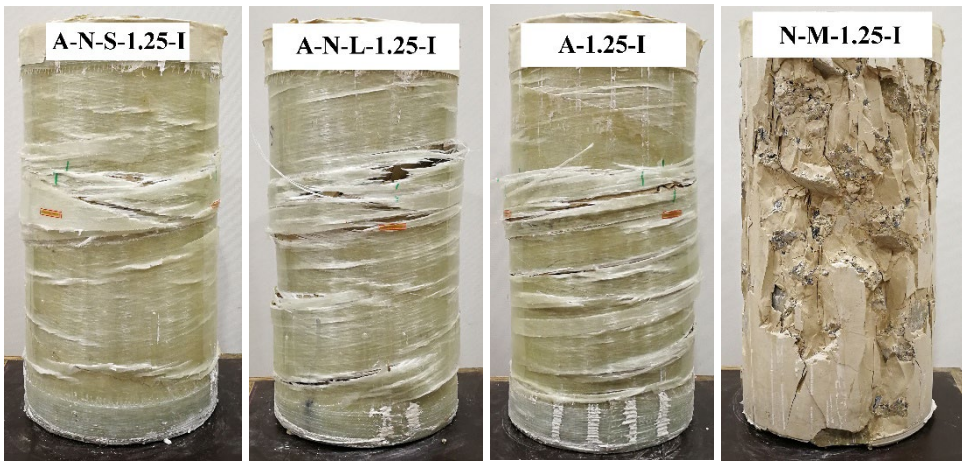

(a) (b) (c) (d)

Figure 11. Typical failure modes of F-R-G, F-G and R-G specimens.

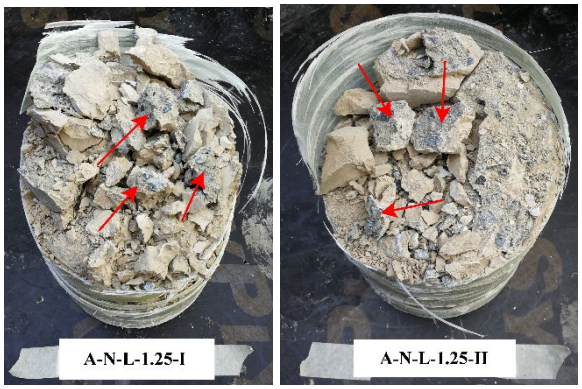

Figure 12. Crushing of normal strength RCLs in F-R-G specimens after test.

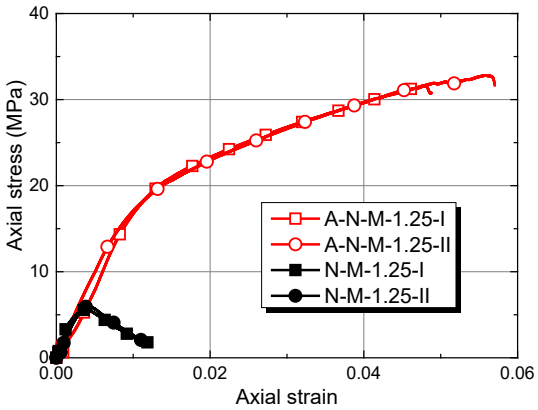

Figure 13. Comparisons of axial stress-strain curves of F-R-G and R-G specimens: effect of FRP confinement.

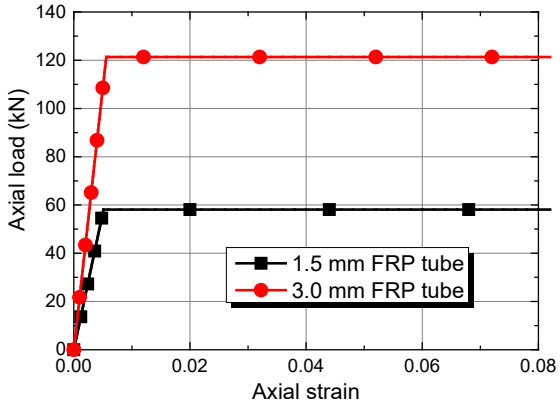

Figure 14. Assumed axial load-strain curves of FRP tubes in F-R-G and F-G specimens.

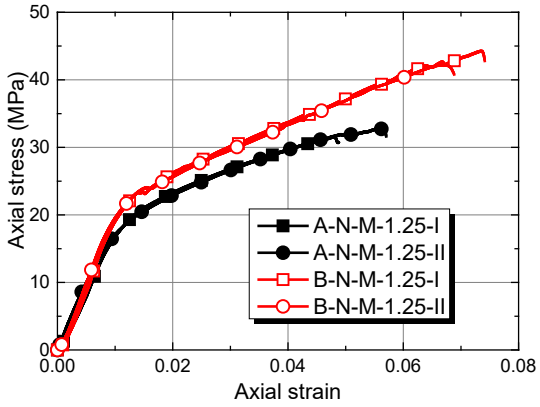

Figure 15. Effect of FRP tube thickness on the axial stress-strain curves of the F-R-G specimens.

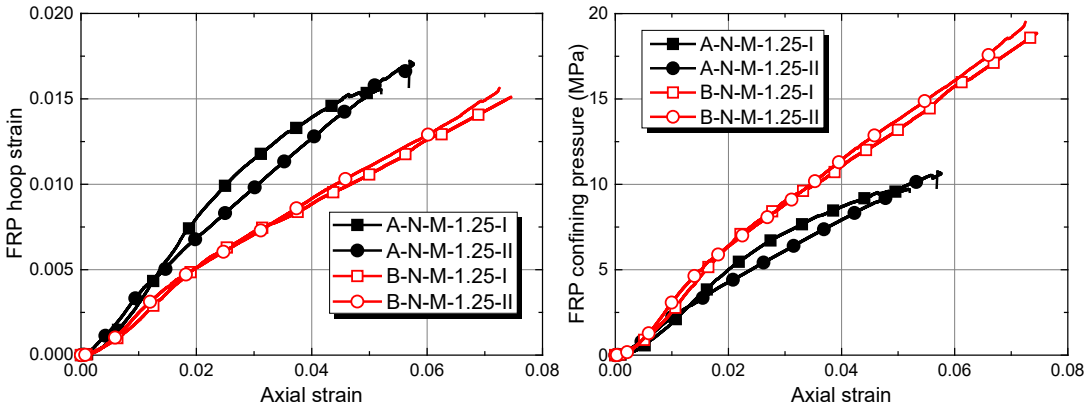

(a) (b)

Figure 16. Effect of FRP tube thickness on (a) FRP hoop strain-axial strain curves and (b) FRP confining pressure-axial strain curves of F-R-G specimens

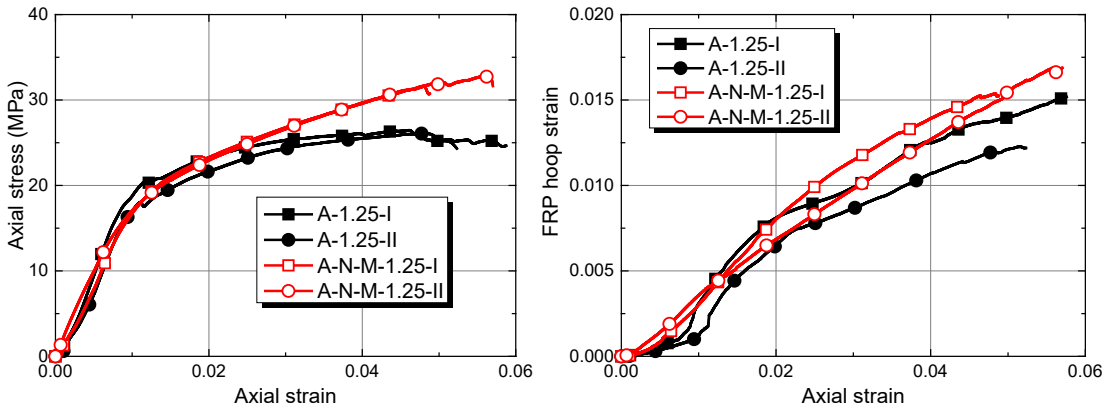

(a) (b)

Figure 17. Effect of the presence of RCLs on the behaviour of F-R-G specimens: (a) axial stress-axial strain curves and (b) FRP hoop strain-axial strain curves.

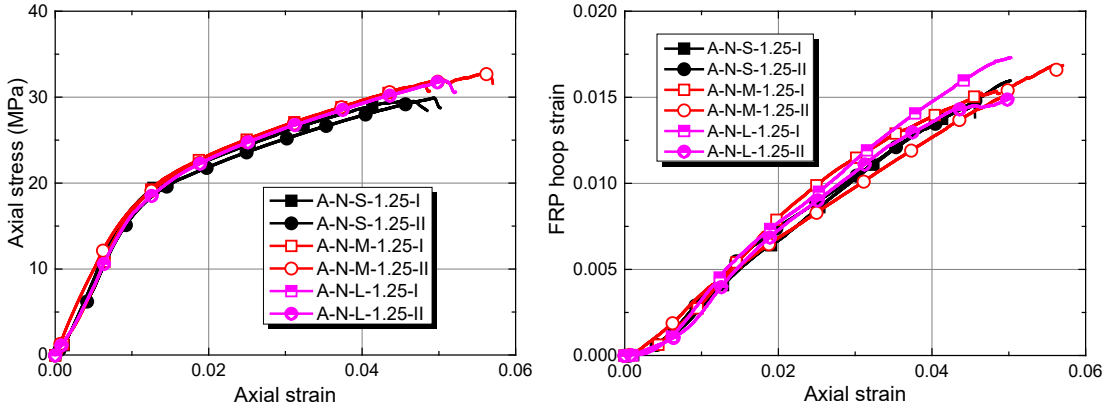

(a) (b)

Figure 18. Effect of the size of RCLs on the behaviour of F-R-G specimens: (a) axial stress strain curves and (b) FRP hoop strain-axial strain curves.

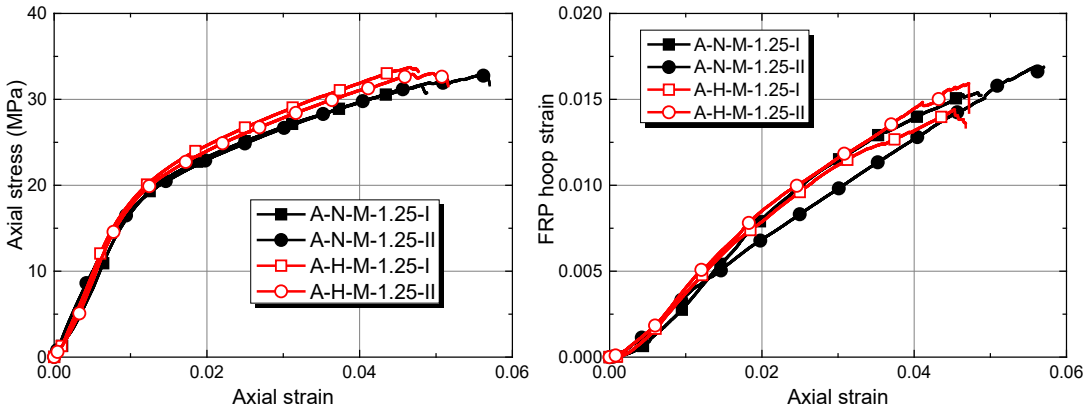

(a) (b)

Figure 19. Effect of the compressive strength of RCLs on the (a) axial stress strain curves and (b) FRP hoop strain-axial strain curves of F-R-G specimens.

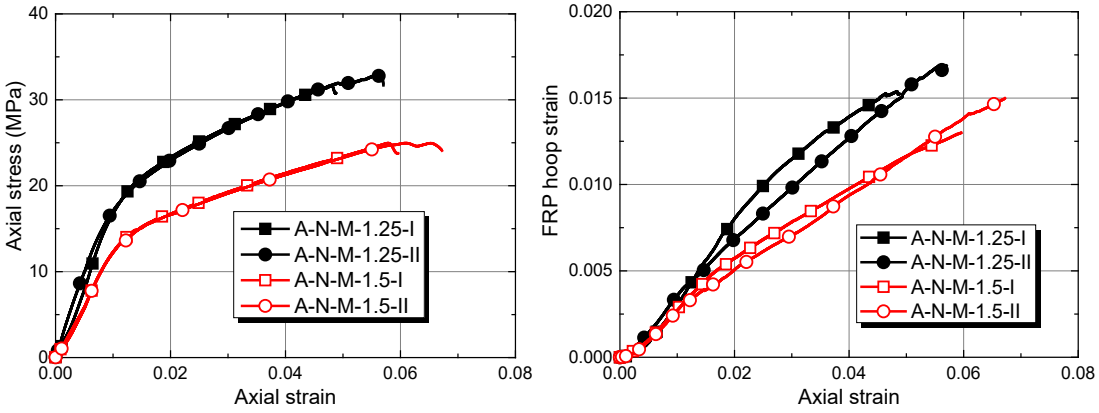

(a) (b)

Figure 20. Effect of WP ratio on the (a) axial stress strain curves and (b) FRP hoop strain-axial strain curves of F-R-G specimens.

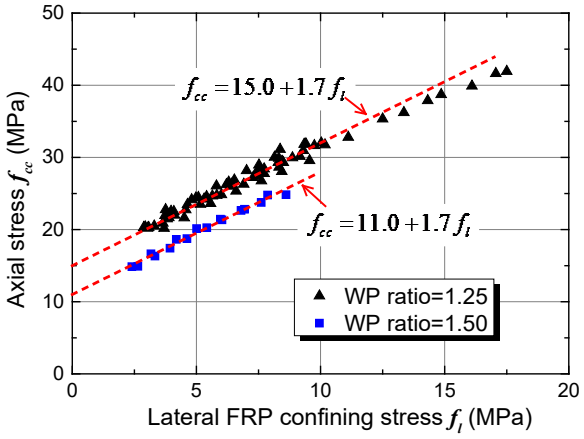

Figure 21. The comparison between the employed database and proposed strength model for the infill material in F-R-G specimens.